Chinese Journal of Aeronautics, (2016), 29(4): 1142–1150

Chinese Society of Aeronautics and Astronautics
& Beihang University

Chinese Journal of Aeronautics

cja@buaa.edu.cn
www.sciencedirect.com

Effect of temperature on corrosion behavior of 3003 aluminum alloy in ethylene glycol–water solution

Chen Xin, Tian Wenming, Li Songmei *, Yu Mei, Liu Jianhua

School of Material Science and Technology, Beihang University, Beijing 100083, China

Received 12 August 2015; revised 12 September 2015; accepted 29 September 2015
Available online 23 December 2015

KEYWORDS

3003 aluminum alloy;
Corrosion behavior;
Electrochemical measurements;
Ethylene glycol;
Temperature

Abstract The effect of temperature on the corrosion behavior of 3003 aluminum alloy in ethylene glycol–water solution was investigated by potentiodynamic polarization and electrochemical impedance spectroscopy (EIS) techniques. The surface characterization was observed and determined by scanning electron microscopy (SEM), atomic force microscopy (AFM) and energy dispersive spectrometer (EDS). The results demonstrate that the anodic aluminum dissolution and the cathodic oxygen reduction were accelerated by the increased temperature. However, as temperature was over 60 °C, the solubility and concentration of oxygen decreased, resulting in the inhibition of cathodic reaction. The cathodic reaction rate of 3003 aluminum alloy rose to the maximum at 60 °C. The Warburg impedance in Nyquist diagram diminished and then was replaced by a negative capacitance caused by the absorption of intermediate corrosion product on electrode. On the other hand, after potentiodynamic measurements, 3003 aluminum alloy suffered pitting corrosion. The dissolution of aluminum alloy around secondary phase particles expanded both horizontally and vertically.

1. Introduction

Aluminum alloys are increasingly used in aerospace industries owing to their excellent properties of high strength-to-weight ratio and good formability.[1–3] For example, the heat exchangers on the aircraft' AC modules are made of the aluminum alloy rather than the other two types of commonly applied materials: the copper alloy and the stainless steel. However, aluminum alloy corrosion occurs and is a major problem in the cooling system of aircraft engine block.[4–6] It is due to a wide temperature range and complex components of coolant to which the aluminum alloy is exposed.[7–9] The appropriate physical and chemical properties of heat coolant have been required to prevent malfunction of cooling system.[10–12] Mixed with water, ethylene glycol is a popular coolant in heat exchanger[13], because of its low cost and excellent freeze and heat-protection over a wide temperature range.[14–17] The main composition of a conventional coolant consists of 30%–70% (by volume) ethylene glycol and some corrosion inhibitors.[18–20] Common heat transfer fluids show a low aggressivity, unless pollution or high-temperature exposure (degradation) occurs.[21] Coolant in the aircraft heat exchanger is always contaminated with chloride ions. In the presence of Cl^-, the

* Corresponding author. Tel./fax: +86 10 82317103.
E-mail address: songmei_li@buaa.edu.cn (S. Li).
Peer review under responsibility of Editorial Committee of CJA.

ELSEVIER Production and hosting by Elsevier

http://dx.doi.org/10.1016/j.cja.2015.12.017

corrosion resistance of aluminum and aluminum alloys decreased significantly and severe pitting corrosion was observed.[22]

3003 aluminum alloy is considered as an advanced material for manufacturing aero heat exchangers.[23–26] It has complex microstructure containing intermetallic particles and impurity precipitation in the aluminum matrix. These particles and precipitation can be either cathodic or anodic with respect to the matrix phase.[27,28] Such complexities have made it challenging to understand the corrosion of 3003 aluminum alloy in cooling systems at different temperatures.

There were a few works in the study of corrosion of aluminum alloys in aqueous ethylene glycol solutions.[29] Liu and Cheng[30] found that the oxide film formed on aluminum depended on the dissolved oxygen in the solution. The cathodic reaction is dominated by the oxygen reduction in aerated solution.[31] In the absence of oxygen, the main cathodic reaction is either reduction of water or reduction of ethylene glycol.[32] However, few of them focused on the effect of temperature on the corrosion behavior of 3003 aluminum alloy in aero coolant systematically. It can provide useful data for material protection and design. In particular, the change in temperature may make a big difference to the inhibition effect of inhibitor. Therefore, it is necessary to study the effect of temperature on the corrosion behavior of 3003 aluminum alloy in the solution.

The present work studies the corrosion and electrochemical behavior of 3003 aluminum alloy in chloride-containing ethylene glycol–water solution at different temperatures by various electrochemical measurements, including corrosion potential, potentiodynamic polarization, cathodic polarization, electrochemical impedance spectroscopy (EIS). The geometrical parameters of pits are measured and analyzed. The surface morphology of aluminum electrode is characterized by scanning electron microscopy (SEM) and atomic force microscopy (AFM). The chemical composition is measured by an energy disperse spectroscopy (EDS) combined.

2. Experimental procedures

2.1. Electrodes and solutions

Test specimens were cut from a 3003 aluminum plate into cylinders of 10 mm diameter, with the chemical composition (wt%): Cu 0.2, Mn 1.5, Fe 0.70, Si 0.60, Zn 0.10, Mg 0.05, Ti 0.05, Cr 0.05 and aluminum in balance. The aluminum electrode was embedded in phenolic resin, leaving a working area of 0.785 cm^2. Electrical contact of the specimen was made from the rear by spot welding a cooper lead on to the back of the specimen. The non-working surface of the electrode was sealed in an epoxy resin. The exposed surface of each electrode was finished by wet-grinding with a series of emery papers from 400 grit to 5000 grit and then cleaned thoroughly with alcohol acetone and deionized water in turn. The base solution was a mixture of 50% ethylene glycol + 50% deionized water + 0.1 $mol \cdot L^{-1}$ NaCl, simulating the aero coolant and the potential chloride contamination. Tests were performed at temperatures ranging from 30–80 °C, consistent with the typical operating temperature in the aero cooling system. The test temperature was maintained through a water bath controlled by a thermoelectric couple. All solutions were made from analytic grade reagents and ultrapure deionized water.

2.2. Electrochemical measurement

Electrochemical measurements were conducted on a three electrode cell with the test specimen as working electrode(WE), a platinum as counter electrode (CE) and a saturated calomel electrode (SCE) as reference electrode (RE). Prior to electrochemical measurement, the specimen was immersed in the static solution for 3 h in order to obtain a steady corrosion potential. Open-circuit potentials were monitored prior to any polarization or impedance measurements.

Potentiodynamic scans were performed at a positive direction from −0.8 V(vs. SCE) to −0.45 V(vs. SCE) with a scan rate of 30 mV/min on Princeton 2273. Polarization stopped when the anodic current density exceeded 0.01 mA. The values of corrosion current density (i_{corr}), corrosion potential (E_{corr}), anodic and cathodic Tafel slops (b_a, b_c) were fitted and calculated through a Zview analytical software. Cathodic polarization was carried out by sweeping from −0.6 V(vs. SCE) negatively to about −1.3 V(vs. SCE).

All the EIS measurements were conducted at open circuit potential on CHI 660E (Hua Chen instrument corporation, Shanghai). Impedances were characterized over the frequency range from 100 kHz to 10 mHz, with the AC signal amplitude being ± 10 mV(vs. SCE). Equivalent circuit modeling was performed using ZsimpWin software.

For each temperature, at least three parallel valid samples were tested to ensure the reproducibility of the results. The sample data closest to the average level was the final data used in analysis. Al the tests were performed open to air without agitation of the electrolyte.

2.3. Surface characterization

After potentiodynamic polarization, the 3003 aluminum electrode was removed from solution. Before AFM measurement the sample was cleaned by ultrasonic bath for 10 min to get rid of corrosion product, rinsed with deionized water and dried with cold air for atomic force microscopy (AFM) analysis. AFM analysis was conducted on a Veeco Dimension Icon operating in Tap Control mode under ambient conditions in air at a scan size of 30 μm × 30 μm to provide detailed topographic information. Images were analyzed by the AFM NanoScope Analysis software, version 1.40. And then a layer of gold was sprayed on the surface of the electrode to enhance the electrical conductivity prior to SEM (scanning electron microscopy) characterization conducted on CamScan3400. The morphological features of different regions of the electrode were characterized by SEM at 2000× magnification. Then, the total number and physical dimensions of pits located in the microscopical view were recorded without repetition. The number of pits was counted on the visual field of the microscopy. We chose ten visual fields of microscopy randomly on each sample under the same magnification, recorded the number of pits on it, and then calculated the number of pits on per mm^2 Elemental composition was measured with a combined EDS (energy dispersive spectrometer) instrument.

3. Presentation of results

3.1. Polarization curve measurements

The corrosion potential of the electrode increased at first and then fluctuated around −0.58 V(vs. SCE) with the immersion time.

Fig. 1 shows the polarization curves of 3003 aluminum electrode measured in the test solution at different temperatures, and T is temperature. It is seen that 3003 aluminum alloy would not be passivated in the ethylene glycol–water solution containing 0.1 mol · L^{-1} NaCl. With the increase of temperature, the corrosion potential of aluminum decreased and anodic dissolution current density increased. Cathodic current density increased until the temperature was up to 60 °C, and then decreased as the temperature reached 80 °C.

The electrochemical parameters, including corrosion current density, corrosion potential, anodic and cathodic Tafel slopes are fitted and listed in Table 1.

Fig. 2 shows the cathodic polarization curves at various temperatures. The characteristic of cathodic polarization curves are similar. The reductive current density decreased rapidly with the positive shift of potential before the curve revealed a knee point after which an approximate plateau showed. Cathodic polarization curve was divided into two parts by the knee point. The part of cathodic curve at potentials more positive than the knee point has been demonstrated in Fig. 2. We deal with the part of cathodic curve at potentials more negative than the knee point. With temperature increasing, the reductive current density increased. Moreover, the knee point shifted positively as temperature increased.

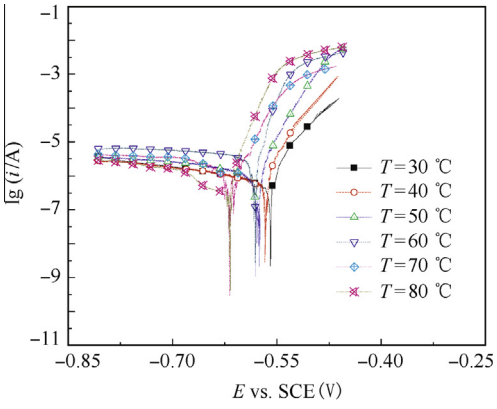

Figure 1 Polarization curves of 3003 aluminum alloy at different temperatures.

Table 1 Fitted electrochemical parameters at different temperatures.

T (°C)	E_{corr} vs. SCE(mV)	i_{corr} (μA · cm^{-2})	b_a vs. SCE (mV)	b_c vs. SCE (mV)
30	−577	0.77	45.9	−317
40	−584	0.92	38.2	−402
50	−585	1.59	31.7	−545
60	−589	2.49	27.5	−656
70	−608	3.87	26.5	−458
80	−618	3.91	19.3	−287

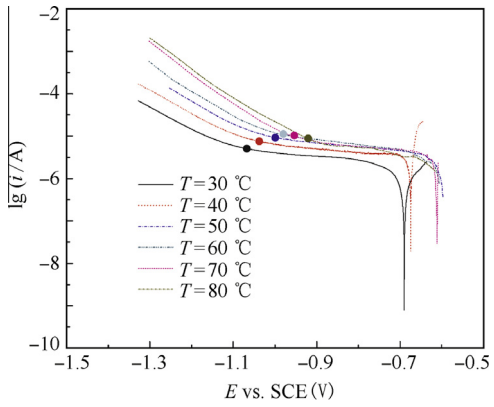

Figure 2 Cathodic polarization curves of 3003 aluminum alloy at different temperatures.

3.2. EIS measurements

Fig. 3 shows the Nyquist diagrams of 3003 aluminum electrode in the aerated test solution at different temperatures. It is seen that in the high-frequency range, all the impedance spectra had an identical characteristic that a depressed semicircle showed and the diameter of the semicircle decreased with the increasing of temperature. In the low-frequency range at temperatures of 30, 40, 50 °C, the measured EIS plots were typically featured with a diffusive tail, a relatively straight line, and became less straight at 60 °C. The diffusive tail of the impedance spectra was replaced by a reversed semicircle at low frequency when the temperature rose to 70 °C and 80 °C. Furthermore, the diameter of the semicircle decreased with the increasing temperature.

3.3. Surface characterization

Figs. 4 and 5 show the SEM images of the surface morphology for 3003 aluminum electrode before and after potentiodynamic polarization in the tested solution at different temperatures.

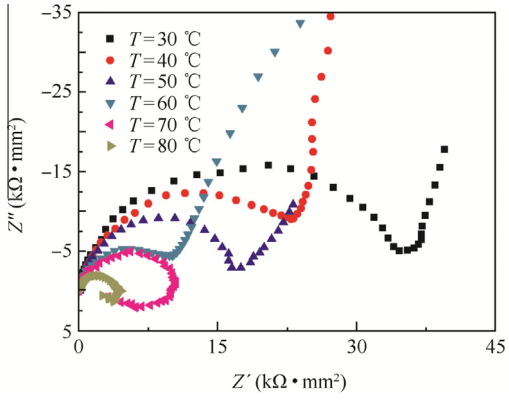

Figure 3 Nyquist diagrams of 3003 aluminum alloy at different temperatures.

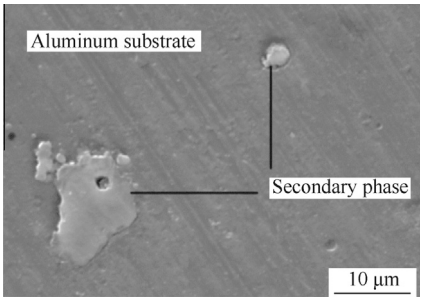

Figure 4 SEM images of surface morphology for 3003 aluminum electrode before polarization (2000×).

The pits were in rounded or elliptic shape. Some of the pits were filled with a particle. A number of particles shaped of stretched ellipses were also observed in the aluminum alloy substrate. The element composition of the stretched-ellipse shaped particle was measured as shown in Table 2, demonstrating that they were secondary phase particles rich in copper and manganese. The number of pits and the size of pit mouth width at different temperatures are shown in Figs. 6 and 7, where P is the percentage of pit mouth width at different temperatures. With temperature rising, pit number tended to decrease, while the pit mouth width increased and pit size distribution was inclined to be scattered.

Topographical changes were qualitatively characterized by AFM three-dimensional (3D) and two-dimensional (2D) images. The 3D and 2D AFM topography images and topographic line-scans through the second phase and the pit are depicted in Fig. 8(a)–(c). Fig. 8(a) depicts the 3D AFM topography image; Fig. 8(c) shows the topographic line-scan results of Fig. 8(b), where H is the coordinates of the vertical direction and L is the coordinates of the horizontal direction of the line-scan. In the 3D image, small hills were present in the places of secondary phase and inverted hills were present in the places of pit. The depth of pits were recorded and 20 pits on the aluminum electrode were recorded at each temperature. The results are shown in Fig. 9(a)–(f). The depth of pits increased

Table 2 Element composition of stretched-ellipse shaped particle.

Element	C	O	Mg	Al	Si	Fe	Mn	Cu
Weight percentage (wt%)	7.83	7.46	0.16	41.53	0.33	0.43	6.25	36.01

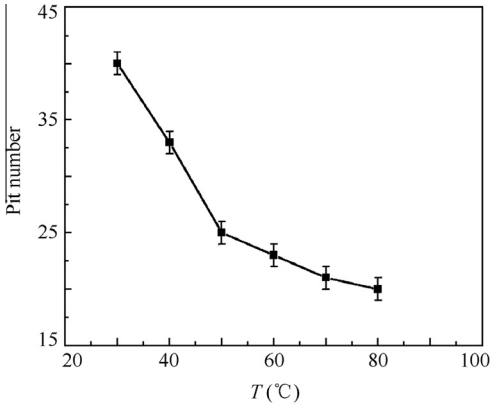

Figure 6 Pit number on the surface at different temperatures.

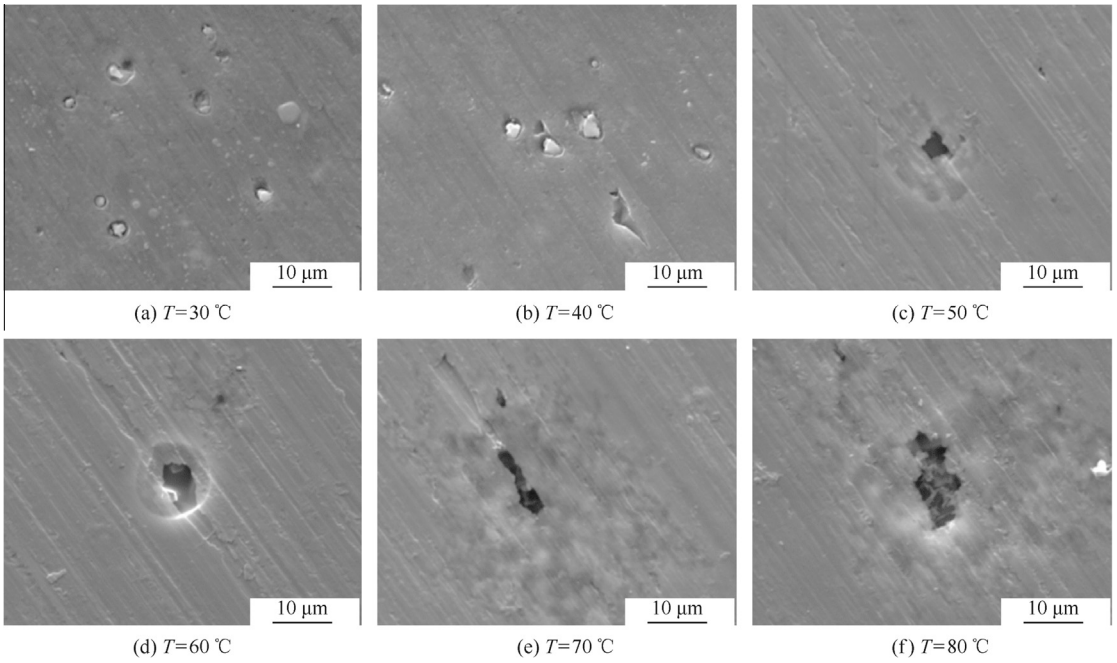

Figure 5 SEM images of surface morphology for 3003 aluminum electrode at different temperatures (2000×).

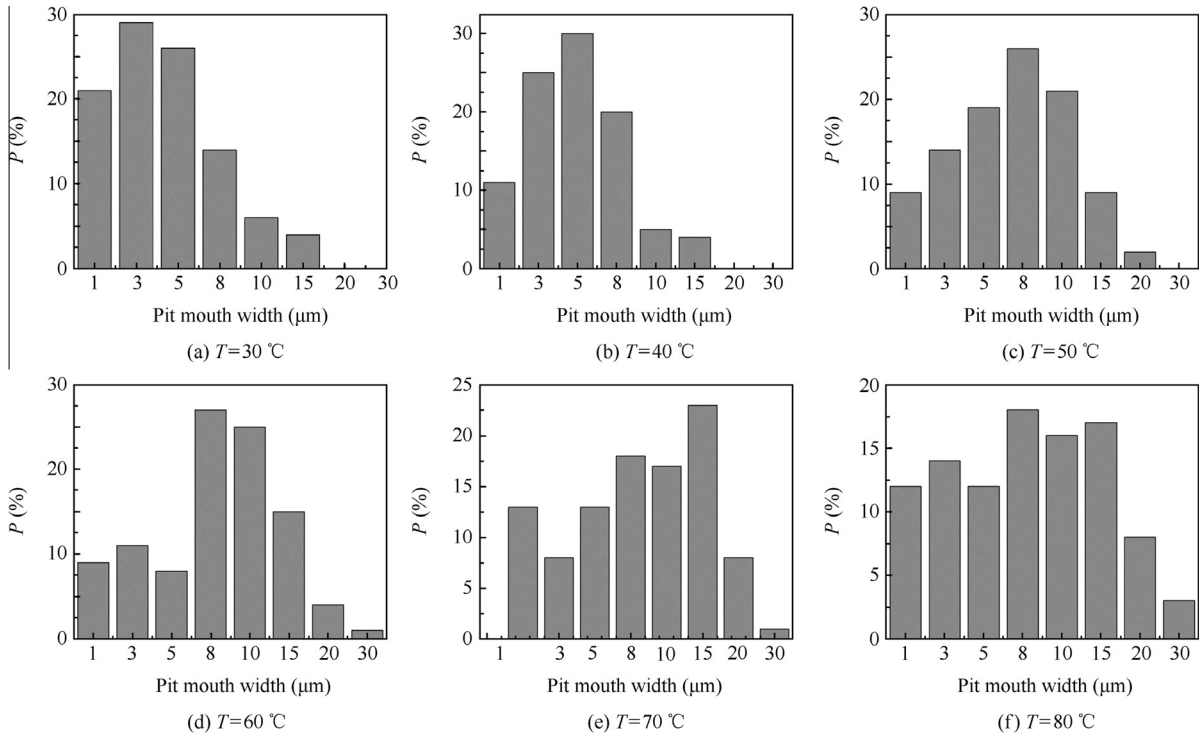

Figure 7 Pit mouth width at different temperatures.

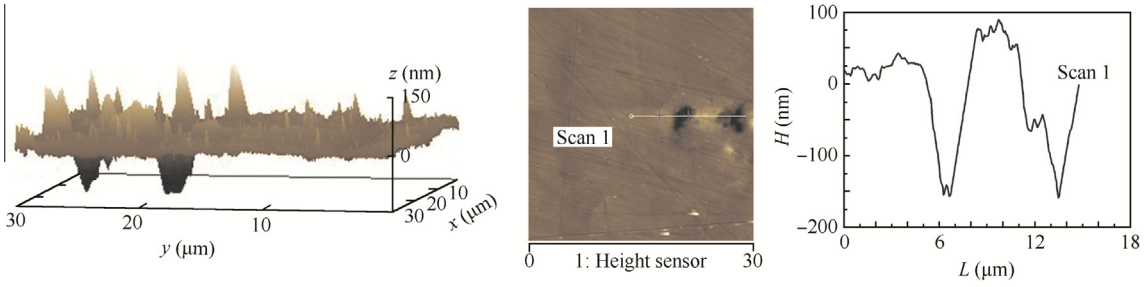

Figure 8 AFM topography images and topographic line-scan through the second phase and pit.

with the increase of temperature. Pits showed a trend of expansion.

4. Discussions

4.1. Effect of temperature on corrosion reaction

Generally, the electrochemical corrosion of aluminum alloy in a near-neutral aqueous solution in the presence of oxygen is characterized by

Cathodic reaction:

$$O_2 + 2H_2O + 4e \rightarrow 4OH^- \quad (1)$$

Anodic reaction:

$$Al \rightarrow Al^{3+} + 3e \quad (2)$$

$$Al^{3+} + 3OH^- \rightarrow Al(OH)_3 \quad (3)$$

In the presence of oxygen, a layer of aluminum oxide film is formed on aluminum surface. Upon the addition of ethylene glycol in the solution, ethylene glycol would be reduced and an aluminum–alcohol can also be formed:

$$CH_2CH_2(OH)_2 + e \rightarrow OHCH_2CH_2O^- + H \quad (4)$$

$$Al^{3+} + 3OHCH_2CH_2O^- \rightarrow Al(OHCH_2CH_2O)_3 \quad (5)$$

The aluminum–alcohol is formed when the oxygen is insufficient.[30] In the absence of oxygen, the main cathodic reaction is either reduction of ethylene glycol by Eq. (4) or reduction of water:

$$H_2O + e \rightarrow H + OH^- \quad (6)$$

Therefore, the resultant film would be a mixture of aluminum oxide and aluminum–alcohol films.[32]

The positive shift of open circuit potential of 3003 aluminum electrode shows the oxidation of the electrode upon the immersion in the solution. The open circuit potential

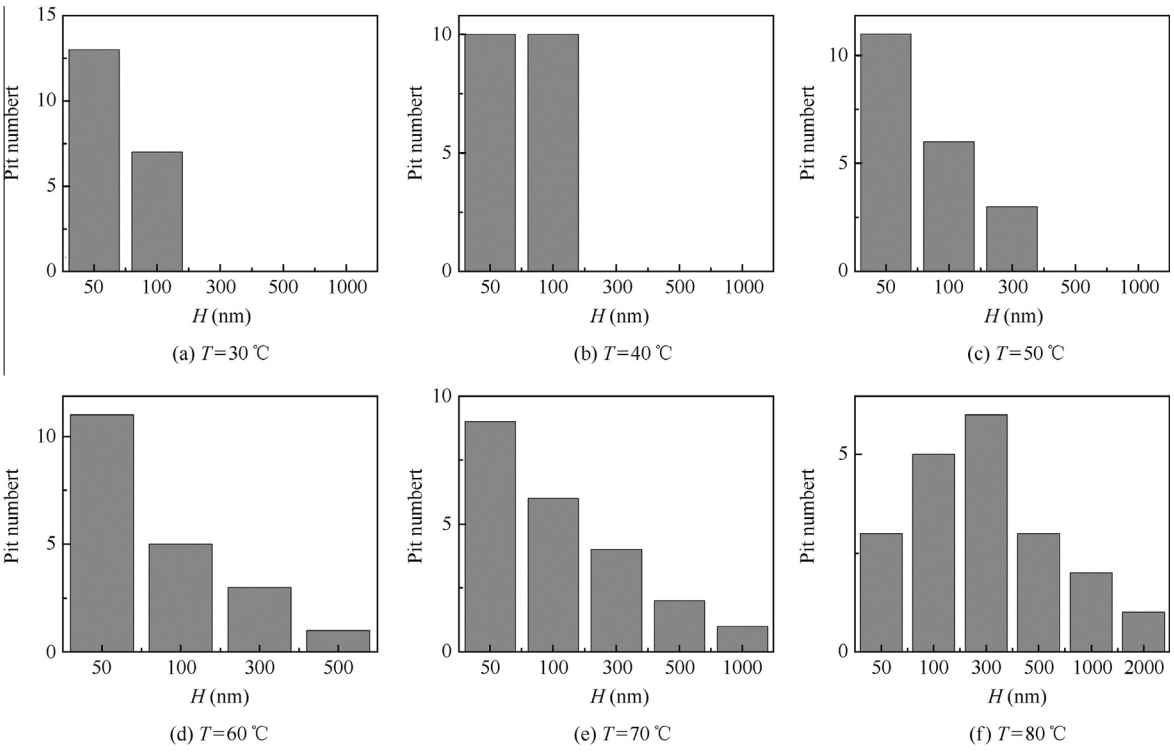

Figure 9 Pit depth at different temperatures.

fluctuated around a specific value, indicating that the film formation and dissolution achieves an equilibrium state.[33,34]

It is seen from Table 1 that the increased temperature shifted E_{corr} negatively. In general, a more negative corrosion potential indicates a more active state. The electrode became more vulnerable to the test solution with the increased temperature, which is associated with a higher anodic dissolution trend. With temperature rising, b_a decreased from 45.9 mV (vs. SCE) to 19.3 mV(vs. SCE). The decrement of b_a showed that the increase in temperature lowered the anodic reaction resistance, and thus accelerated anodic dissolution. Apparently, the increase in temperature significantly activated the 3003 aluminum. b_c decreased from −317 mV(vs. SCE) to −656 mV(vs. SCE) and then increased to −287 mV(vs. SCE). It indicated that the cathodic reaction was accelerated with temperature rising until temperature was up to 60 °C. And when temperature was higher than 60 °C, the cathodic reaction rate slowed down.

With the increase of temperature, the anodic reaction rate of 3003 aluminum was accelerated while the cathodic reaction rate increased at first then decreased, which indicated that the corrosion mechanism of 3003 aluminum would be changed at higher temperature.

The effect of temperature on corrosion reaction basically complies with the Arrhenius equation:

$$k = A\exp(-E_a/RT) \tag{7}$$

where k is reaction speed constant, A pre-exponential factor, E_a apparent activation energy, R molar gas constant and T thermodynamic temperature.

k determines the inherent reaction speed of a reaction. It can be seen from the Arrhenius equation, in the premise that E_a remains unchanged and temperature range is limited, the reaction speed constant increases with the increase of temperature, and so is the reaction speed. The corrosion-related interfacial reaction process is accelerated with the elevated temperature. Moreover, an elevated temperature lowers the reaction activation energy at the same time. The anodic reaction, dissolution of aluminum tends to be easier to occur, and so does the cathodic reaction. Both the anodic and cathodic reaction accelerated due to the elevated temperature. Therefore, the anodic and the cathodic current density increase with the increasing temperature to a certain extent. Thus, the corrosion reaction rate is accelerated which is identified by i_{corr}.

On the other hand, the cathodic reaction is a purely diffusion-controlled process within a certain potential region in aerated ethylene glycol–water solution.[35,36] It is dominated by the diffusion and the reduction of dissolved oxygen. With temperature rising, the coefficient of diffusion oxygen molecules increases and the viscosity of ethylene glycol would decrease,[37] which resulted in the acceleration of oxygen diffusion and thus the increase of cathodic reductive current density. However, as the temperature of solution kept growing, the solubility of oxygen decreased, thus the concentration of dissolved oxygen decreased. There was not sufficient oxygen for cathodic reduction reaction. The decrease of the content of oxygen weakens the cathodic reaction, leading to the decrement of cathodic current density and the increase of b_c, as shown in Fig. 2 and Table 1. Here, the electrochemical dissolution of 3003 aluminum alloy is limited by the cathodic reduction of oxygen with diffusion control. The cathodic reaction rate of 3003 aluminum alloy rose to the maximum at 60 °C.

As the cathodic reaction went, the dissolved oxygen reacted and the oxidation of aluminum electrode persisted. As the content of dissolved oxygen became less and less, the reduction of ethylene glycol or water which refers to the curve at potentials

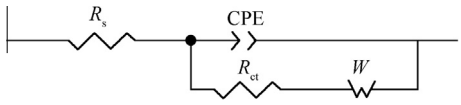

Figure 10 Equivalent circuits for fit of experimental data.

more negative than the knee point in Fig. 3, became prominent. The reduction of ethylene glycol and water was enhanced by the increasing temperature, since its reaction active energy was lower and its reaction speed constant was larger at higher temperature. As a result, the cathodic current density increased with the rising temperature monotonously. The knee point shifting positively as temperature increased provided evidence for the less content of oxygen at higher temperature.

4.2. Effect of temperature on EIS plots

To further determine the electrochemical corrosion mechanism of aluminum alloy in ethylene glycol–water solution at different temperatures, EIS measurements and analyses were performed (see Fig. 4). The observed "diffusive tail" in the low frequency range at lower temperature represents the Warburg impedance and is the typical characteristic of the corrosion process where diffusion of oxygen is involved.[38,39] It indicates that mass-transfer step plays an important role in electrode process. The diffusive Warburg impedance tended to diminish with the increasing temperature. When temperature was higher than 60 °C, the Warburg impedance characteristics almost disappeared. This provides evidence to demonstrate that the corrosion mechanism of 3003 aluminum is already changed with the increase of temperature. Technically, the slopes of diffusive tails are not strict 45°, which is because of the intermediate reaction during corrosion parallel to the oxygen diffusion[34,35] or the non-stationary conditions under measurement.[40]

The electrochemical equivalent circuit shown in Fig. 10 was used for fitting EIS data with diffusive impedance. To simulate the "dispersion effect" and compensate for the electrode non-homogeneity such as the rough electrode surface, a constant phase element (CPE) is used in the circuit to replace the ideal double-layer capacitance. A CPE's impedance (Z_{CPE}) is given by

$$Z_{CPE} = \frac{(j\omega)^{-n}}{Y_0} \tag{8}$$

where ω is angular frequency and Y_0 constant. n is the frequency dispersion factor, which varies from 1 to 0 generally. When $n = 1$, CPE can be considered an ideal capacitance; when $n = 0$, it is a resistance.[41]

Simulations by means of the circuit provide a good agreement with the experimental data at different temperatures. Fig. 11 shows a typical example to compare the fitted results with the experimental data by both Bode and phase angle diagrams, where R_s is solution resistance, CPE constant phase element, R_{ct} charge-transfer resistance and W Warburg impedance. It is seen that the selected equivalent circuit models fit the experimental data very well. The values of the fitted equivalent circuit elements are listed in Table 3.

In the Nyquist diagram, charge transfer resistance (R_{ct}) is a characteristic quantity for an electrode reaction and has a critical influence on the inherent speed of interfacial charge transfer reaction.[38,42] The value of R_{ct}, shown as Table 3, basically decreases with the elevated temperature, indicating an enhanced destabilization of electrode upon the increase of temperature. It is attributed to the enhanced oxygen diffusion and aluminum oxidation. The value of Warburg impedance

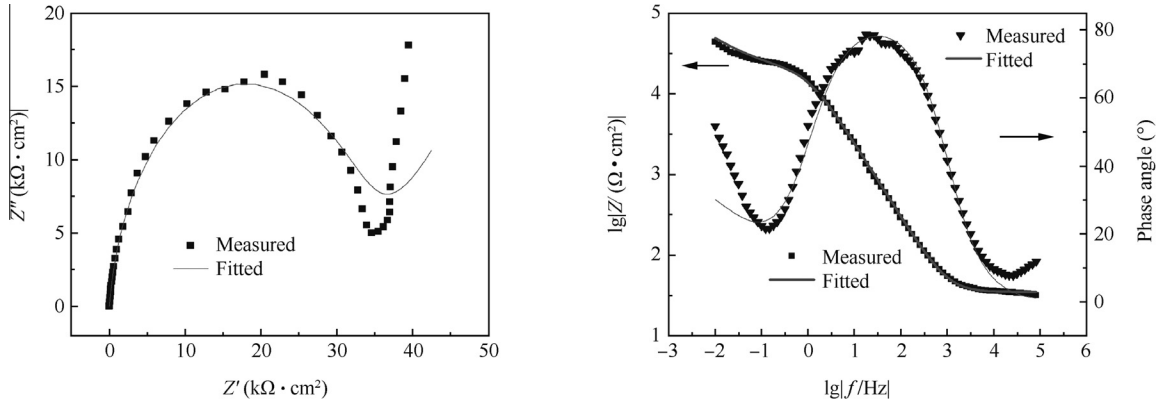

Figure 11 EIS Nyquist plot and Bode plot of aluminum electrode at 30 °C.

Table 3 Values of fitted equivalent circuit elements.

T (°C)	R_s (Ω · cm²)	Y_0 (Ω^{-1} · cm^{-1} · s^{-n})	n	R_{ct} (Ω · cm²)	W (Ω · cm² · s^{-5})	CHI^2
30	41.07	7.68×10^{-6}	0.9112	33,500	2928	0.0049
40	34.82	8.95×10^{-6}	0.9208	20,020	1179	0.0106
50	38.01	9.33×10^{-6}	0.9221	16,475	107	0.0165
60	39.6	1.11×10^{-5}	0.9297	8633	10.01	0.0140

decreases with the rising temperature, agreed with analyzed. It should be mentioned that the fitting results, values of fitted equivalent circuit elements should only be considered in a form of indirect changes of electric parameters, rather than direct values because of the possible non-stationarity of the system and high level of CHI^2 error during the fitting procedure.

As temperature increased to 70 °C, instead of the diffusive impedance, a reversed semicircle emerged in the low frequency range. The emergence of reversed semicircle is attributed to either a high electrode surface roughness or an absorption effect of intermediate corrosion product.[43,44] It is studied by Liu and Cheng[32] that when Cl^- concentration is up to 0.01 M($0.1\ mol \cdot L^{-1}$) and 0.1 M($0.5\ mol \cdot L^{-1}$), the content of intermediate products adsorbing in aluminum–alcohol film is significant. Therefore, the observed reversed semicircle mainly results from the absorption of intermediate corrosion product on electrode. Equivalent circuits used in calculating the impedance of electrochemical adsorption systems are better to be negative capacitance. The existing devices designed for impedance optimization lack equivalent circuits involving the negative capacitance, thus the equivalent circuit for impedance including reversed semicircle is not given.[45]

Aluminum corrosion reaction is mixed-controlled by activation step and mass-transfer step through the anodic film in ethylene glycol–water solution.[44] As temperature rose, the diffusive impedance feature faded away. Therefore, mass-transfer step became less dominant in the electrode reaction process, resulting in the change of Nyquist diagram and electrochemical equivalent circuit.

4.3. Surface morphology

According to the surface characterization, after the potentiodynamic measurements the aluminum electrode suffered pitting corrosion. Pit nucleation was associated with the active points and the local dissolution of aluminum alloy substrate around the secondary phase particles. The stretched second phase particles are primarily intermetallics rich in copper and manganese. Corrosion is known to initiate preferentially at the particle–matrix interface.[43] There actually existing an effect which is called micro-galvanic coupling between secondary phase particles and the aluminum matrix resulting in preferential dissolution of aluminum alloy.[3,43] Intermetallic particles acted as local cathodes in the corrosion process. Pits formed when aluminum dissolved and intermetallic particles detached from the aluminum matrix. At higher temperature, aluminum alloy substrate had a higher dissolution activity, the active dissolution of aluminum was enhanced and the dissolved area of aluminum was larger. The micro-galvanic coupling effect was enhanced. The dissolution of aluminum alloy expanded both horizontally and vertically (see Figs. 7 and 9). The adjacent pits converged to form a larger pit, which would cause the decrement of the amount of pits under different temperatures. As a consequence, the size of pit was enlarged and the aluminum electrode had a trend of uniform corrosion.

It is commonly acknowledged that the corrosion of aluminum under certain environment is determined by the specific corrosion process.[41] In the solution of ethylene glycol–water containing $0.1\ mol \cdot L^{-1}$ NaCl, the elevated temperature can affect the corrosion process mainly from two aspects: one is that it accelerates the electrochemical reaction (both anodic and cathodic) and determines the diffusion process of reaction species towards the reaction sites; the other is that it affects the size and expansion of pits. Larger and deeper pits are formed at higher temperature, and a trend of uniform corrosion is presented.

5. Conclusions

(1) An increase of experimental temperature would accelerate the 3003 aluminum alloy corrosion rate in ethylene glycol–water solution containing $0.1\ mol \cdot L^{-1}$ NaCl. The dissolution of aluminum shows a feature of accelerated with the rise of temperature. The elevated temperature enhances the diffusion of oxygen and accelerated cathodic reaction rate. However, as temperature kept rises, the solubility and concentration of oxygen decrease, resulting in the inhibition of cathodic reaction. The cathodic reaction rate of 3003 aluminum alloy rises to the maximum at 60 °C. Overall, the elevated temperature accelerates the anodic and cathodic reaction speed and facilitates the corrosion reaction to a certain extent.

(2) On the other hand, with the increase in temperature, the Warburg impedance in Nyquist diagram diminishes and a reversed semicircle caused by the absorption of intermediate corrosion product on electrode emerges. The mass-transfer step of corrosion becomes less dominant in the electrode reaction process.

(3) After potentiodynamic measurements, 3003 aluminum alloy suffers pitting corrosion. At higher temperature, the micro-galvanic coupling effect between secondary phase particles and the aluminum matrix is enhanced. The adjacent pits converge to form a larger pit, thus the active dissolution of aluminum is enhanced and the dissolved area of aluminum is larger. The pit corrosion process is promoted by both horizontal and vertical expansion of pit.

Acknowledgment

This study was co-supported by the National Natural Science Foundation of China (No. 51271012).

References

1. Abiola OK, Otaigbe JOE. Effect of common water contaminants on the corrosion of aluminum alloys in ethylene glycol–water solution. *Corros Sci* 2008;**50**(5):242–7.
2. Yang B, Gershun AV, Woyciesjes PM. Controlled atmosphere brazing of aluminum heat exchangers and effects of flux residues on corrosion of the cooling system components in engine coolants. *Fuel* 2009;**15**(2):2099–115.
3. Sakairi M, Sasaki M, Kaneko A, Seki Y, Nagasawa D. Evaluation of metal cation effects on galvanic corrosion behavior of the A5052 aluminum alloy in low chloride ion containing solutions by electrochemical noise impedance. *Electrochim Acta* 2014;**131**(3):123–9.
4. Thomson JK, Pawel SJ, Wilson DF. Susceptibility of aluminum alloys to corrosion in simulated fuel blends containing ethanol. *Fuel* 2013;**111**(1):592–7.
5. David JK, Paul L. Evaluation of heat exchanger surface coatings. *Appl Therm Eng* 2010;**30**(2):2333–8.

6. Wang Q, Yan PG, Dong P, Feng GT, Wang ZQ. Application of coolant diffusion equation in numerical simulation of flow in air-cooled turbine. *Chin J Aeronaut* 2012;**25**(4):566–74.
7. Himpel G, Herrmann M, Hohn S. Comparison of high-temperature corrosion of aluminum nitride, alumina, magnesia and zirconia ceramics by coal ashes. *Ceram Int* 2015;**41**(5):8288–98.
8. Niu L, Cheng YF. Erosion–corrosion of aluminum alloys in ethylene glycol–water solutions in absence and presence of sand particles. *Corros Eng Sci Technol* 2009;**44**(5):389–93.
9. Su JX, Ma MY, Wang TJ, Guo XM, Hou LG, Wang ZP. Fouling corrosion in aluminum heat exchanger. *Chin J Aeronaut* 2015;**28**(3):954–60.
10. Seifzadeh D, Bashranavaz H. Corrosion protection of AZ91 magnesium alloy in cooling systems. *Trans Nonferrous Met Soc China* 2013;**23**(1):2577–84.
11. Bustos ES, Rodriguez JGG, Uruchurtu J, Bravo VMS. Corrosion behavior of iron-based alloys in the LiBr + ethylene glycol + H_2O mixture. *Corros Sci* 2009;**51**(3):1107–14.
12. Park IJ, Nam TH, Kim JH, Kim JG. Evaluation of corrosion characteristics of aluminum alloys in the bio-ethanol gasoline blended fuel by 2-electrode electrochemical impedance spectroscopy. *Fuel* 2014;**126**(5):26–31.
13. Ranjbar K, Abasi A. Failure assessment of crude oil preheating tubes in mono ethylene glycol–water mixture solution. *Eng Fail Anal* 2013;**31**:161–7.
14. Weon JI. Corrosion mechanism of aluminum alloy by ethylene glycol-based solution. *Mater Corros* 2013;**64**(1):50–9.
15. Tadjamoli M, Tzinmann M, Fiaudc C. Galvanic corrosion of the aluminum-copper couple in uninhibited aqueous solutions of glycols. *Br Corros J* 1984;**19**(1):36–40.
16. Monticelli C, Brunoro G, Zucchi F, Fagiolif F. Inhibition of localized attack on the aluminum alloy AA 6351 in glycol/water solutions. *Mater Corros* 1989;**40**(3):393–8.
17. Wang XY, Wang JM, Wang QL, Shao HB, Zhang JQ. Effect of polyethylene glycol (PEG) as an electrolyte additive on the corrosion behavior and electrochemical performances of pure aluminum in an alkaline zincate solution. *Mater Corros* 2011;**62**(2):1149–52.
18. Vigdorovivh VI, Tsygankova LE. Corrosion of aluminum in sulfate ethylene glycol solutions. *Corros Sci* 1993;**13**(2):215–22.
19. Khomami MN, Danaee I, Attar AA, Peykari M. Corrosion of alloy steel in 30% ethylene glycol solution and Cr O_4^{2-} under hydrodynamic condition. *J Iron Steel Res Int* 2013;**20**(6):82–7.
20. Fekry AM, Fatayerji MZ. Electrochemical corrosion behavior of AZ91D alloy in ethylene glycol. *Electrochim Acta* 2009;**54**(4):22–8.
21. Monticelli C, Brunoro G, Frignani A. Corrosion behavior of the aluminum alloy AA 6351 in glycol/water solutions degraded at elevated temperature. *Mater Corros* 1988;**39**(4):379–84.
22. Wong D, Swette L. Aluminum corrosion in uninhibited ethylene glycol–water solutions. *Electrochem Soc* 1979;**126**(1):11–5.
23. Yazdzad AR, Shahrabi T, Hosseini MG. Inhibition of 3003 aluminum alloy corrosion by propargyl alcohol and tartrate ion and their synergistic effects in 0.5% NaCl solution. *Mater Chem Phys* 2008;**109**(2):199–205.
24. Dehoff RR, Babu SS. Characterization of interfacial microstructures in 3003 aluminum alloy blocks fabricated by ultrasonic additive manufacturing. *Acta Mater* 2010;**58**(2):4305–15.
25. Majed MR, Carlberg T. Solidification studies of 3003 aluminium alloys with Cu and Zr additions. *J Mater Sci Technol* 2011;**27**(7):615–27.
26. Solange Y, Dugarte P, Benjamin HP. Statistical analysis of the optical interferometry of pitting process in aluminum 3003 sheets exposed to saline environment. *Proc Mater Sci* 2015;**8**(6):82–90.
27. Zhou W, Aung NN, Choudhary A, Kanouni M. Heat-transfer corrosion behavior of cast Al alloy. *Corros Sci* 2008;**50**(3):3308–13.
28. Hughes AE, Markley TA, Garcia SJ, Mol JMC. Comparative study of protection of AA 2024-T3 exposed to rare earth salts solutions. *Corros Eng Sci Technol* 2014;**49**(6):674–87.
29. Zaharieva J, Milanova M, Mitov M, Lutov L, Manev S, Todorovsky D. Corrosion of aluminum and aluminum alloy in ethylene glycol–water mixtures. *J Alloy Compd* 2009;**470**(1):397–403.
30. Liu Y, Cheng YF. Characterization of passivity and pitting corrosion of 3003 aluminum alloy in ethylene glycol–water solutions. *J Appl Electrochem* 2011;**41**(1):151–9.
31. Trombetta F, Souza FR, Souza MO, Borges BC, Panno AF, Martini EMA. Stability of aluminum in 1-butyl-3-methylimidazolium tetra fluoroborate ionic liquid and ethylene glycol mixtures. *Corros Sci* 2011;**53**(1):51–8.
32. Liu Y, Cheng YF. Effects of coolant chemistry on corrosion of 3003 aluminum alloy in automotive cooling system. *Mater Corros* 2010;**61**(7):574–8.
33. Bazeleva NA, Herasymenko YS. Corrosion-electrochemical behavior of aluminum alloys in aqueous ethylene glycol media. *Mater Sci* 2007;**43**(6):851–60.
34. Niu L, Cheng YF. Electrochemical characterization of metastable pitting of 3003 aluminum alloy in ethylene glycol–water solution. *Mater Sci* 2007;**42**(2):8613–7.
35. Niu L, Cheng YF. Cathodic reaction kinetics and its implication on flow-assisted corrosion of aluminum alloy in aqueous ethylene glycol solution. *J Appl Electrochem* 2009;**39**(6):1267–72.
36. Zhang GA, Xu YL, Cheng YF. Investigation of erosion–corrosion of 3003 aluminum alloy in ethylene glycol–water solution by impingement jet system. *Corros Sci* 2009;**51**(1):283–90.
37. Xu LY, Cheng YF. Electrochemical characterization and CFD simulation of flow-assisted corrosion of aluminum alloy in ethylene glycol–water solution. *Corros Sci* 2008;**50**(3):2004–10.
38. Martin FJ, Cheek GT, Grady WE, Natishan PM. Impedance studies of the passive film on aluminum. *Corros Sci* 2005;**47**(7):3187–201.
39. Conde A, Damborenea JD. An electrochemical impedance study of a natural aged Al–Cu–Mg alloy in NaCl. *Corros Sci* 1997;**39**(1):295–303.
40. Orlikowski J, Ryl J, Jarzynka M, Krakowwiak S, Darowicki K. Instantaneous impedance monitoring of aluminum alloy 7075 corrosion in borate buffer with admixed chloride ions. *Corrosion* 2015;**71**(7):828–38.
41. Scully JR, Silverman DC, Kengding MW. Electrochemical impedance: analysis and interpretation. *Corros Sci* 1993;**21**(3):128–32.
42. Zhang GA, Xu YL, Cheng YF. Mechanistic aspects of electrochemical corrosion of aluminum alloy in ethylene glycol–water solution. *Electrochim Acta* 2008;**53**(5):8245–52.
43. Feriky AM, Fatayerji MZ. Electrochemical corrosion behavior of AZ91D alloy in ethylene glycol. *Electrochim Acta* 2009;**54**(1):6522–8.
44. Niu L, Cheng YF. Synergistic effects of fluid flow and sand particles on erosion–corrosion of aluminum in ethylene glycol–water solutions. *Wear* 2008;**265**(1):367–74.
45. Elkin VV, Marshako AI, Rybkina AA, Maleeva MA. Interpretation of the impedance comprising negative capacitance and constant phase elements on iron electrode in weakly acidic media. *Russ J Electrochem* 2011;**47**(2):147–58.

Chen Xin is a postgraduate at school of material science and engineering, Beihang University. His main research interests are material science and engineering and material corrosion.

Li Songmei is a professor and Ph.D. supervisor at school of material science and engineering, Beihang University. She received the Ph.D. degree from the same university. Her current research interests are material science and engineering and material corrosion.